

DIAGENETIC EVOLUTION OF SEAMOUNT PHOSPHORITE

LAURA M. BENNINGER*

Geology Department, University of California, Davis, California, 95616, USA

AND

JAMES R. HEIN**

U.S. Geological Survey, MS 999, 345 Middlefield Rd., Menlo Park, California, 94025, USA

ABSTRACT: Phosphorite, limestone, basalt, and breccia/conglomerate occur on the flanks of central Pacific Cretaceous seamounts. Phosphatization occurred during the Tertiary, at or immediately below the sediment-water interface, within thin bodies of porous carbonate sediment and within all rock types that occur on the seamounts. The phosphorites are composed of carbonate fluorapatite (CFA), which lines pores and replaces carbonate and silicate protoliths; protolith fabric is locally preserved in fine detail. Phosphatization is typically most pervasive adjacent to pores, fractures, and the outer surfaces of samples.

In order of decreasing abundance, diagenetic minerals associated with seamount phosphorites (SMP) include: CFA, Fe-Mn oxyhydroxides, palagonite, smectite, phillipsite, and barite. This mineral assemblage indicates that CFA formed under conditions consistent with low-temperature, open-circulation seafloor alteration of basalt. The common association between CFA and precipitation of Fe-Mn oxyhydroxides indicates that SMP formed under oxic to suboxic conditions.

Phosphatization is characterized by mineralization fronts; the angular superposition of those fronts (successive mineralizing fluids coming from different directions) locally leads to irregularly shaped domains that differ in pervasiveness of phosphatization, degree of fabric preservation, and abundance of secondary minerals. Phosphatization is, therefore, controlled by a variety of factors including protolith mineralogy and fabric, degree of pore-fluid saturation with respect to CFA, rate of pore-fluid/seawater circulation (rock-water ratio), and number of previous episodes of phosphatization.

INTRODUCTION

Despite the widespread occurrence of phosphorite on seamounts (Baturin, 1982; Cullen and Burnett, 1986; Burnett et al., 1987; Bersenev et al., 1990; Hein et al., 1993), little is known about the distribution, petrology, or genesis of these unique deposits. Study of sedimentary marine phosphorite has traditionally focused on large, economically important deposits such as the Permian Phosphoria Formation, and on contemporary continental margin deposits such as those forming off the Peru-Chile margin. As a result, current phosphogenic models are based on the study of organically rich deposits that formed in highly productive environments of intense and continuous upwelling. In contrast, seamount phosphorites (SMP) occur in moderate- to low-productivity, organically poor settings (Hein et al., 1993; mean organic carbon content (TOC) is 0.12%); consequently, it is unlikely that upwelling-based models fully explain seamount phosphogenesis.

Recent discoveries of phosphatic nodules and hardgrounds from organic-poor settings, such as those along the east Australian margin, have led to the recognition that phosphogenesis within low-productivity environments may be more widespread than previously thought (O'Brien and Heggie, 1988; O'Brien et al., 1990). Studies of those deposits suggest that bacterial mediation and redox cycling of Fe-Mn oxyhydroxides may be crucial mechanisms for concentrating phosphorus during formation of phosphorite in nonupwelling zones (Jarvis, 1992; Schaffer, 1986; Lucas and Prévôt, 1985). Through the study of mid-Pacific SMP, we evaluate the broad applicability of these mechanisms to phosphogenesis within moderate- to low-productivity environments.

SMP predominantly formed during two time periods in the

Cenozoic, one spanning the Eocene-Oligocene boundary and the other spanning the Oligocene-Miocene boundary (Hein et al., 1993; J. R. Hein and L. H. Chan, unpublished data, 1997). Other, however less extensive, episodes of phosphogenesis also occurred at various times during the Cenozoic. Compositional and paragenetic analyses preclude a hydrothermal origin for these phosphatized (carbonate and volcanic) rocks and sediments. Additionally they indicate that phosphatization occurred under fluctuating oxic/suboxic conditions (Hein et al., 1993). These results suggest that even though the depositional settings of seamount phosphorites contrast with phosphorites from other low-productivity settings, the geochemical constraints on their formation are similar.

In this paper the term seamount is used to describe submarine highs that include seamounts, guyots, ridges, and edifices that support atolls. Phosphorite is used as a general term and is

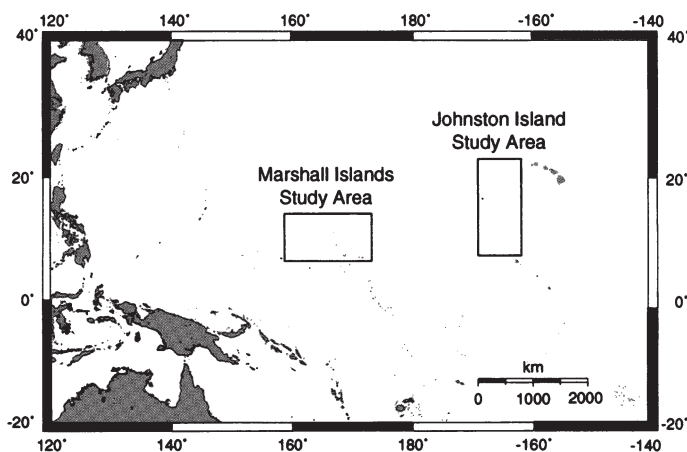


FIG. 1.—Locations of Johnston Island and Marshall Islands regions, central Pacific.

*email: benninger@geology.ucdavis.edu

**email: jhein@octopus.wr.usgs.gov

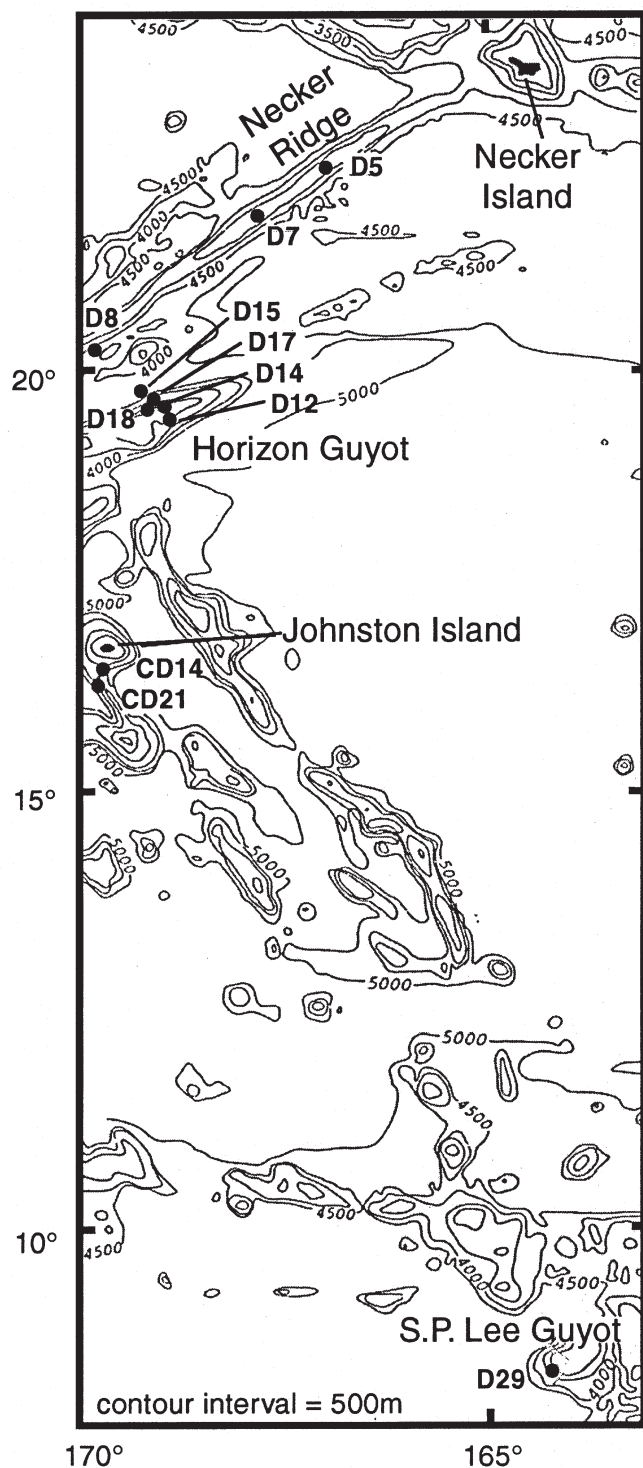


FIG. 2.—Bathymetry of the Johnston Island region showing locations of dredge stations (filled circles).

not meant to imply an economic value for these deposits. The terms replacement and alteration are used interchangeably to describe dissolution of one mineral and precipitation of another in its place. These terms are not meant to imply replacement or alteration through molecular or ionic substitution.

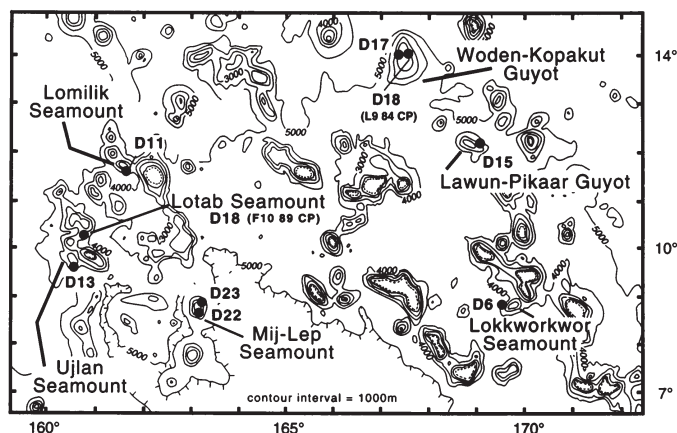


FIG. 3.—Bathymetry of the Marshall Islands region showing locations of dredge stations (filled circles).

METHODS AND SAMPLES

This study is based on thin section examination of 28 phosphorite samples dredged from 10 equatorial Pacific seamounts (Fig. 1; Table 1). Seventeen samples are from the Johnston Island region (Fig. 2) and 11 are from the Marshall Islands region (Fig. 3). This suite of samples was selected as representative of the hundreds of Pacific seamount phosphorite samples that were collected by U.S. Geological Survey chain-bag dredge operations over an 8-year period (1983-1991). Samples from the Johnston Island region were collected from water depths between 1750 m and 4800 m and those from the Marshall Islands region were taken from depths between 1000 m and 2900 m (Table 1). Water depths of most samples are accurate to within 100 m because of short dredge intervals. Generally, prior to dredging, single-channel seismic profiles, 10 kHz bathymetry, and 3.5 kHz sub-bottom profiles were taken; during dredging, the latter two systems were in operation. Shipboard navigation used the Global Positioning System (GPS) and Rhorho, a software program that allows direct ranging on Loran C.

Mineralogy of powdered samples was determined using an X-ray diffractometer (XRD) with $\text{CuK}\alpha$ radiation and curved-crystal carbon monochromator. Petrographic analyses of doubly polished thin sections (0.3 mm thick) were conducted under transmitted and reflected light. Selected thin sections were subsequently carbon coated to 200Å and then analyzed with a scanning electron microscope (SEM) with back-scattered electron (BSE) capabilities and an X-Ray analyzer (EDS).

DEPOSITIONAL SETTING

SMP occur on seamounts in the Indian, Atlantic, and Pacific Oceans (Baturin, 1982), and are apparently most abundant within equatorial Pacific regions. A compilation of SMP occurrences reported in the literature indicates that deposits range in latitude from 26°N to 33°S, while most occur at latitudes between 8°N and 26°N (Benninger, 1998).

Nearly all equatorial Pacific seamounts host at least minor occurrences of phosphorite. Phosphorites were recovered from about 90% of the approximately 100 equatorial Pacific

TABLE 1.—SAMPLE DESCRIPTIONS AND LOCATIONS

Sample	Edifice	Latitude (on & off bottom)	Longitude (on & off bottom)	Depth (m)	General Thin Section Description
L5 83 HW					
D5-A3-1	Necker Ridge	22° 18.98' 22° 18.30'	166° 53.93' 166° 54.12'	2350–2100	Phosphatized, poorly sorted, breccia-conglomerate with crust of Fe-Mn oxyhydroxides.
D5-A3-10	Necker Ridge	22° 18.98' 22° 18.30'	166° 53.93' 166° 54.12'	2350–2100	Phosphatized, poorly sorted, breccia-conglomerate cemented by phosphatized foraminiferal carbonate.
D5-A3-11	Necker Ridge	22° 18.98' 22° 18.30'	166° 53.93' 166° 54.12'	2350–2100	Phosphatized volcanoclastic breccia encrusted by Fe-Mn oxyhydroxides.
D5-A3-12	Necker Ridge	22° 18.98' 22° 18.30'	166° 53.93' 166° 54.12'	2350–2100	Intensely phosphatized volcanoclastic breccia overlain by ~1.5 cm of phosphatized limestone.
D5-A3-15	Necker Ridge	22° 18.98' 22° 18.30'	166° 53.93' 166° 54.12'	2350–2100	Moderately altered vesicular basalt encrusted by Fe-Mn oxyhydroxides. Vesicles in zeolitized and phosphatized basalt are partly to completely filled by carbonate fluorapatite (CFA).
D5-A3-18	Necker Ridge	22° 18.98' 22° 18.30'	166° 53.93' 166° 54.12'	2350 - 2100	Phosphatized and brecciated glassy basalt encrusted by Fe-Mn oxyhydroxides. Fe-Mn oxyhydroxide crust supports pebbles of phosphatized basalt and phosphatized breccia-conglomerate.
D7-A1	Necker Ridge	21° 47.89' 21° 48.01'	167° 37.41' 167° 36.92'	2100	Partly phosphatized and palagonitized brecciated glassy basalt with crust of Fe-Mn oxyhydroxides.
D8-A4	Necker Ridge	20° 12.57' 20° 11.88'	169° 30.36' 169° 31.15'	4800–4500	Fe-Mn oxyhydroxide nodule with a nucleus of phosphatized carbonate mudstone.
D12-A10	Horizon Guyot	19° 22.4' (on bottom)	168° 41.69' (on bottom)	2000	Phosphatized, poorly-sorted, glassy basalt breccia encrusted by ~0.75 mm of Fe-Mn oxyhydroxides.
D14-A2	Horizon Guyot	19° 30.19' (on bottom)	168° 46.67' (on bottom)	1800–1750	Intensely phosphatized volcanoclastic breccia with CFA matrix and crust of Fe-Mn oxyhydroxides.
D14-A6	Horizon Guyot	19° 30.19' (on bottom)	168° 46.67' (on bottom)	1800–1750	Palagonitized basalt with 1 cm thick crust of Fe-Mn oxyhydroxides. Thin (0.5 mm) layer of phosphatized foraminiferal carbonate separates Fe-Mn oxyhydroxides from basalt substrate.
D15-B1	Horizon Guyot	19° 41.64' 19° 40.54'	168° 59.647' 168° 59.02'	4500–4300	Fe-Mn oxyhydroxide encrusted phosphatized limestone containing phosphatic peloids, altered hyaloclastite fragments, rare phosphorite, fish fragments, and Fe-Mn oxyhydroxide crust fragments.
D17-A1	Horizon Guyot	19° 33.20' (on bottom)	168° 49.94' (on bottom)	2400	Non-vesicular basalt clast with thin palagonite rim overlain by layered phosphatized limestone and encrusted by porous Fe-Mn oxyhydroxides.
D18 B3-7	Horizon Guyot	19° 30.89' 19° 29.69'	168° 51.28' 168° 51.91'	1799–1780	Phosphatized non-vesicular basalt overlain by 2-3 mm of Fe-Mn oxyhydroxides and topped by partly phosphatized foraminiferal limestone.
D29 1A-A	S.P. Lee Guyot	8° 17.82' 8° 18.69'	164° 22.11' 164° 21.04'	1400	Phosphatized planktonic foraminiferal grainstone in which CFA lines and partly fills molds of sand- to silt-sized foraminiferal tests.
L9 84CP					
D6-2	Lokkwo- kwo	8°45.28' (on bottom)	169° 49.53' (on bottom)	2900	Intensely phosphatized breccia-conglomerate encrusted by Fe-Mn oxyhydroxides.
D6-3	Lokkwo- kwo	8° 45.28' (on bottom)	169° 49.53' (on bottom)	2900	Moderately phosphatized clastic breccia overlain by 1.5 cm of phosphatized foraminiferal wackestone and encrusted by Fe-Mn oxyhydroxides.
D6-15C	Lokkwo- kwo	8° 45.28' (on bottom)	169° 49.53' (on bottom)	2900	Partly phosphatized foraminiferal limestone encrusted by 2 mm of Fe-Mn oxyhydroxides.
D15-4	Lawun- Pikaar	12° 10.97' 12° 12.71'	168° 59.74' 168° 58.30'	1000–1300	Partly phosphatized foraminiferal wackestone with abundant disseminated Fe-Mn oxyhydroxides and encrusted by porous Fe-Mn oxyhydroxides.
D17-2	Woden- Kopakut	13° 54.28' 13° 54.24'	167° 37.64' 167° 38.25'	1600	Phosphatized massive foraminiferal limestone encrusted by Fe-Mn oxyhydroxides.
D18 3B-B	Woden- Kopakut	13° 53.98' (on bottom)	167° 39.22' (on bottom)	1600	Moderately altered basalt clast with common fractures infilled by phosphatized foraminiferal-rich carbonate and locally lined by smectite.

TABLE 1.—(CONTINUED)

Sample	Edifice	Latitude (on & off bottom)	Longitude (on & off bottom)	Depth (m)	General Thin Section Description
F10 89 CP					
D11-3E	Lomilik	11° 37.0' 11° 39.0'	161° 41.1' 161° 39.8'	1870–1465	Phosphatized volcanoclastic siltstone with interlaminae of volcanoclastic mudstone.
D13-3A (2)	Lotab	09° 37.2' 09° 37.3'	160° 32.6' 160° 33.0'	2130–2280	Phosphatized breccia-conglomerate containing phosphatized clasts encrusted by Fe-Mn oxyhydroxides. Within phosphatized carbonate matrix, CFA-rich and CFA-poor regions are separated by sharp, irregular boundaries that locally cross-cut foraminifera tests.
D18-1C	Lotab	10° 15.5' 10° 15.15'	160° 40.4' 160° 40.7'	1975–1940	Partly phosphatized foraminiferal wackestone.
D22-1A	Mij-Lep	08° 43.7' 08° 43.6'	163° 11.4' 163° 12.9'	1270–1245	Fe-Mn oxyhydroxide crust containing common voids, possibly burrows. Phosphatized carbonate lines and fills some voids.
D22-1C	Mij-Lep	08° 43.7' 08° 43.6'	163° 11.4' 163° 12.9'	1270–1245	Phosphatized hyaloclastite with sparse phosphatized pumice clasts and glassy basalt fragments.
D23-6	Mij-Lep	08° 52.0' 08° 51.7'	163° 10.3' 163° 10.6'	1405–1305	Phosphatized basalt breccia encrusted by Fe-Mn oxyhydroxides.
F7 86 HW					
CD 14-2B	S. Johnston Island Ridge	16° 26.8' 16° 26.2'	169° 32.3' 169° 33.6'	2530–2340	Phosphatized foraminiferal mudstone
CD 21-7-2	S. Johnston Island Ridge	16° 26.6' 16° 27.2'	169° 31.7' 169° 31.8'	2550–2370	Non-vesicular basalt encrusted by 3.5 cm of Fe-Mn oxyhydroxides.

seamounts that were dredged over a 10-year period, and the estimated overall mean phosphorus content is 2.3% P (5.2% P_2O_5) for those deposits (Hein et al., 1993). Some equatorial areas, including the Johnston Island and Marshall Islands areas, appear to be especially phosphorite rich, with from 5% to >25% CFA within 60–70% of all rocks dredged (Hein et al., 1993).

Dredge and drill core recoveries indicate that SMP occurs at, or immediately below, the sediment-water interface. Drill core from the Emperor Seamount Chain contains phosphatic grains and fracture fillings in the uppermost 2 m of core (Jackson et al., 1980) and core from Resolution Guyot, Mid Pacific Mountains, contains phosphorite within 15 cm of the seafloor (Sager et al., 1993). Moreover, while phosphorite was recovered many meters below the seafloor at both Allison Guyot in the Mid Pacific Mountains (Sager et al., 1993) and Wodejebato Guyot in the Marshall Islands (Premoli-Silva et al., 1993), those phosphorites co-occur with Fe-Mn oxyhydroxide crusts, implying formation within a few meters of the paleo-sediment-water interface.

SMP occurs preferentially on seamount flanks (Hein et al., 1990, 1993) and the deposits are not concentrated within any particular water depth interval. SMP is also found on seamount summits (Sager et al., 1993; Premoli-Silva et al., 1993) and redeposited SMP is found within turbidite and debris flows (Sager et al., 1993). Preferential occurrence of SMP on seamount flanks (rather than summits) may reflect phosphogenesis during times when seamount summits were emergent and therefore unavailable to phosphate-rich seawater. Alternatively,

rapid sedimentation rates on seamount summits may have precluded phosphatization. In addition, SMP formation is likely associated with the oxygen minimum zone (Benninger, 1998), which generally intersects the seamount flanks rather than their summits.

In the Marshall and Johnston Islands areas, seamounts exhibit from 3 km to 5 km of relief and have moderately steep flanks that vary in slope from 9° to 27° (Kayen et al., 1989; Hein et al., 1990). Seamount flanks, which host most SMP deposits, are generally draped by volcanoclastic breccias and conglomeratic limestones. Typically, flanks are free of fine-grained sediment except for local sediment ponds. Seamount summits range from rugged, sediment-starved basaltic ridge tops to terraced platforms covered by up to 200 m of fine-grained carbonate sediment locally interbedded with volcanoclastic talus (Schwab et al., 1988; Hein et al., 1990).

SEAMOUNT PHOSPHORITE LITHOTYPES

SMP are classified here according to protolith type since phosphorites form through alteration of preexisting seamount rocks and sediments. In approximate order of decreasing abundance, CFA occurs as an authigenic pore-lining phase and/or diagenetic replacement within three main rock types: 1) volcanoclastic breccia-conglomerate, 2) limestone, and 3) basalt; these are described in detail below. To a lesser extent, CFA also

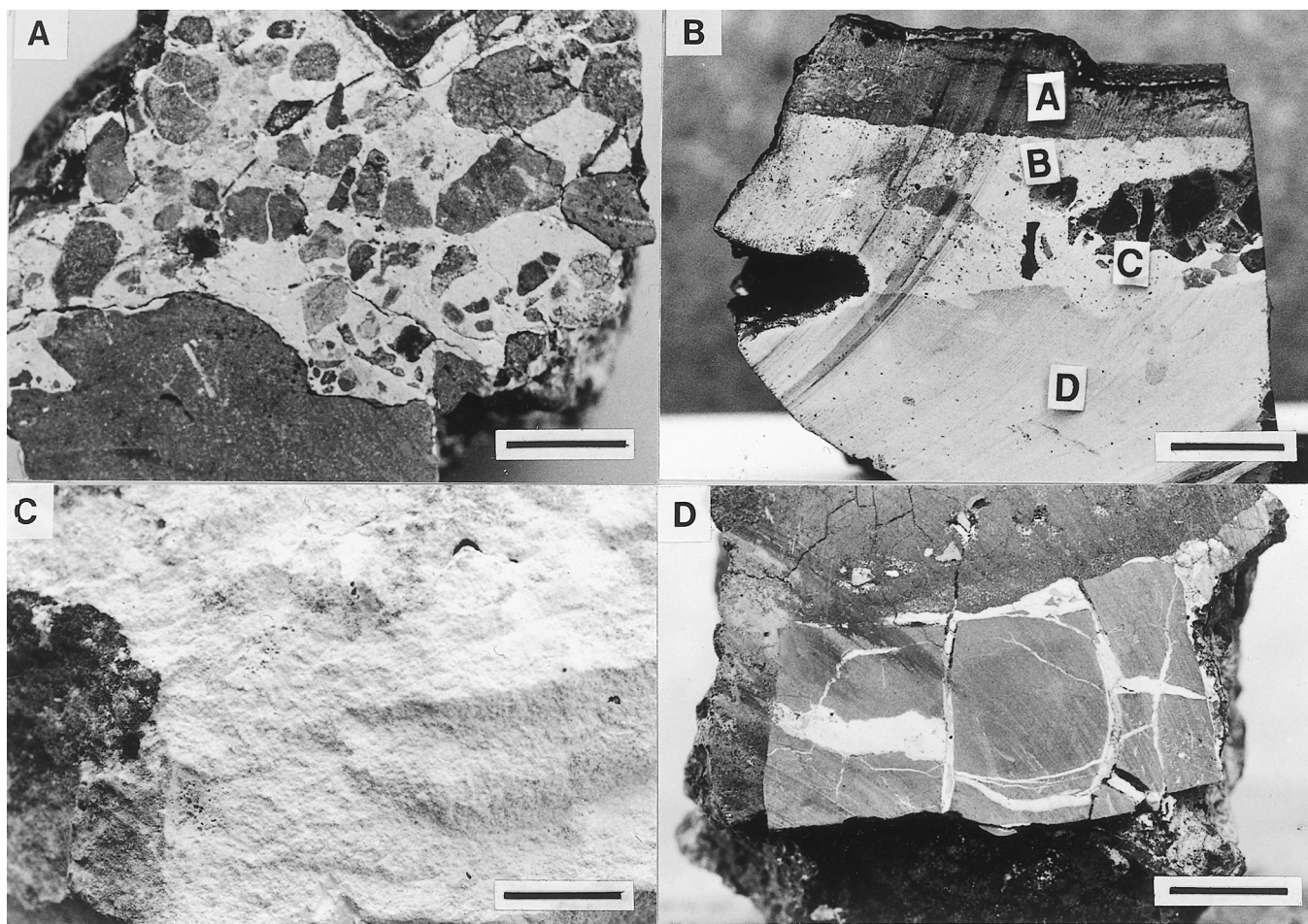


FIG. 4.—A) Volcaniclastic breccia-conglomerate containing partly to completely phosphatized lithic fragments within a matrix (light gray) of CFA-replaced, massive, foraminiferal limestone. Angular and subrounded clasts are very poorly sorted; grains range from cobble- (bottom of photo) to silt-sized. A thin (< 0.5 cm) Fe-Mn oxyhydroxide crust (black) covers the upper surface of the rock. *F10-89-CP D19-3*. Scale bar = 2 cm. B) Bedded phosphatic foraminiferal- and nannofossil-rich wackestone. In layers A and D, cryptocrystalline CFA (locally intergrown with dendritic Fe-Mn oxyhydroxides) supports abundant molds of foraminifera and nannofossil tests. Layer A is topped by 1 cm of Fe-Mn oxyhydroxides (black) with phosphatic interlayer (light gray). Within layers B and C, CFA matrix supports pebble- to silt-sized intraclasts of volcaniclastic breccia-conglomerate, partly to unaltered basalt and glassy basalt, Fe-Mn oxyhydroxide crust fragments, and phosphorite. Burrows are present in layer D and along contact between layers D and C. *L9-84-CP D6-3*. Scale bar = 2 cm. C) Massive, completely phosphatized foraminiferal grainstone. CFA cement surrounds sand-sized foraminifera molds and minor silt-sized nannofossil molds. Patina of Fe-Mn oxyhydroxides (black) encrusts outer surface of sample (left). *L5-83-HW D29-A1-A*. Scale bar = 2 cm. D) Massive phosphatized basalt (light gray) with common fractures and minor vugs filled by phosphatized detrital carbonate (white). Basalt groundmass is locally CFA-replaced. Basalt block is topped by 4-cm thick Fe-Mn oxyhydroxide crust (darker gray) that contains common vugs filled with geopetal CFA-replaced foraminiferal limestone (dark cream). *L9-84-CP D18-3*. Scale bar = 2 cm.

lines and/or replaces: 4) detrital carbonate within fractures and vugs, 5) detrital carbonate within Fe-Mn oxyhydroxide crusts or separating crusts from substrate, and 6) preexisting phosphorite. Rare CFA of possible hydrothermal origin is also suggested by rare veins lined by CFA, phillipsite, and barite. Hydrothermal SMP from the central Pacific were previously identified by oxygen isotope analyses (Hein et al., 1993).

Phosphatized Volcaniclastic Breccia-Conglomerate

Most SMP occurs within volcaniclastic breccia-conglomerate, and secondarily within volcaniclastic sandstone, volcaniclastic siltstone, and hyaloclastite. This group of phosphatized clastic rocks (hereafter referred to as volcaniclastic breccia-conglomerate) typically contains partly to completely

phosphatized lithic fragments within a matrix of partly to completely CFA-replaced, massive, foraminiferal limestone (Fig. 4A). Angular to rounded clasts are commonly encrusted by Fe-Mn oxyhydroxide layers (patina to 3 cm) and are typically poorly sorted; clasts range up to cobble size. Commonly, large fragments are grain-supported and smaller clasts are matrix-supported.

Lithic fragments within phosphatized breccia-conglomerate largely consist of vesicular glassy basalt (containing minor plagioclase, pyroxene, and/or olivine microphenocrysts), and non-vesicular glassy basalt (containing abundant plagioclase micro-laths and minor pyroxene micro-phenocrysts). To a lesser extent, clasts also include preexisting phosphorite, limestone, glass shards, and Fe-Mn oxyhydroxide crust fragments. Minor broken plagioclase laths, fish debris, and ironstone are locally

present. The abundance of preexisting phosphorite is poorly known because of the difficulty in distinguishing between preexisting phosphorite clasts and clasts phosphatized after inclusion within breccia-conglomerate. The abundance of volcanic glass is also poorly known because highly altered glass shards are difficult to distinguish from massive, CFA-replaced limestone matrix.

Phosphatized Limestone

The second most abundant SMP rock type consists of massive to well-bedded phosphatized foraminifera- and nannofossil-rich wackestone (Fig. 4B), packstone, and rare grainstone (Fig. 4C). Cryptocrystalline CFA matrix (commonly intergrown with dendritic Fe-Mn oxyhydroxides) supports intraclasts and foraminifera and nannofossil tests that are typically represented as molds. In decreasing order of abundance, intraclasts are composed of extensively altered glassy basalt and hyaloclastite, fresh to partly altered basalt and glassy basalt, Fe-Mn oxyhydroxide crust fragments, and phosphorite. Rarely, intraclasts also include fish debris, euhedral barite, plagioclase, and pyroxene. Vugs within phosphatized limestones are commonly lined by Fe-Mn oxyhydroxides.

Within bedded phosphatized limestone (Fig. 4B), millimeter- to centimeter-thick layers are distinguished by differences in allochem and intraclast abundance, degree of phosphatization, and differences in crystallinity of the CFA matrix. Soft-sediment deformation features (including flame structures and convolute laminae) are locally present. Rarely, layers are separated by laminated Fe-Mn oxyhydroxides.

Phosphatized Basalt

The third most abundant protolith is composed of either plagioclase-phyric Hawaiite with abundant randomly oriented

plagioclase microlites, minor Ti-rich clinopyroxenes, minor Fe-Ti oxides, and minor olivine; or alkalic basalt with sparse olivine, clinopyroxene, and plagioclase phenocrysts. Massive to vesicular phosphatized basalt is typically encrusted by Fe-Mn oxyhydroxides (1 mm-3 cm thick). Within phosphatized basalts CFA lines vugs; replaces basalt groundmass; and replaces vug, void, and fracture-filling detrital carbonate (Fig. 4D).

PARAGENESIS OF SEAMOUNT PHOSPHORITE

Paragenetic diagrams are presented for phosphatized volcanic material (Fig. 5) and phosphatized limestone (Fig. 6). A separate paragenetic diagram is not presented for phosphatized breccia-conglomerates because those rocks reflect phosphatization processes and paragenetic histories that are characteristic of both phosphatized volcanic rocks and limestone. The paragenetic sequences are generalized from observation of many thin sections and do not necessarily represent mineralization sequences observed in all samples. Unidentified and rarely occurring phases are not included in the paragenetic diagrams.

Phosphatization of Volcanic Material

Numerous workers (Alt, 1995; Thompson, 1983; Honnorez, 1981) reported that open-circulation, low-temperature alteration of basalt is typified by early dissolution and/or palagonitization of glass, followed by partial replacement of volcanic material by zeolites, smectites, and Fe oxides. Thin-section and SEM analyses presented below indicate that this same sequence of diagenetic alteration and replacement operates within phosphatized seamount volcanic material (Fig. 5).

As discussed in detail in the following section, phosphatization of volcanic material occurs through lining of vugs and fractures by CFA, smectite, zeolite, and Fe-Mn oxyhydroxides, and through replacement of volcanic material by intergrown CFA,

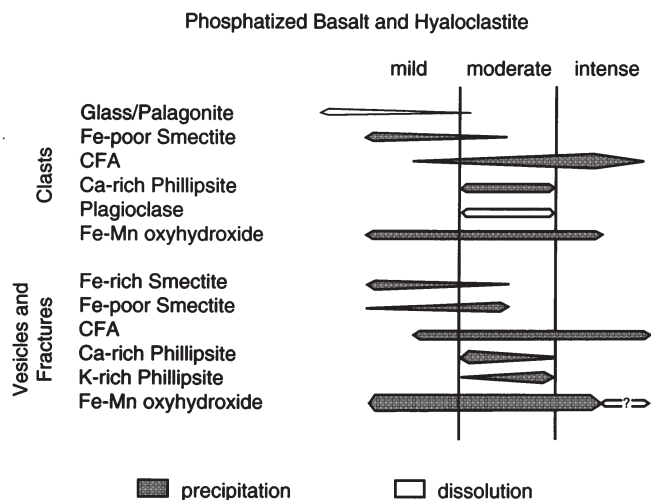


FIG. 5.—Paragenetic diagram for phosphatization of volcanic material. Thickness of bars is schematically proportional to degree of mineralization.

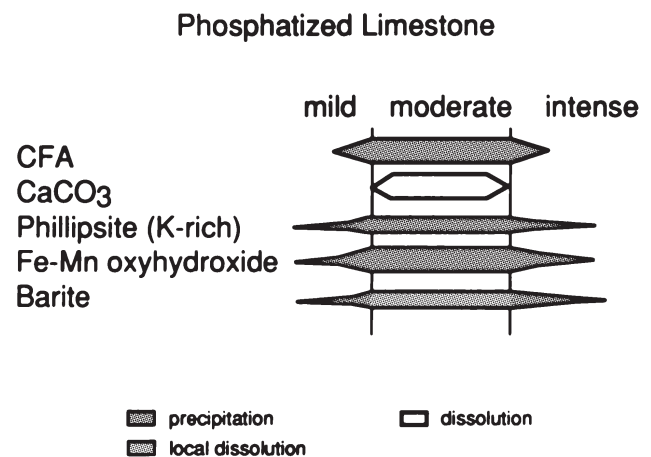


FIG. 6.—Paragenetic diagram for phosphatization of limestone. Thickness of bars is schematically proportional to degree of mineralization.

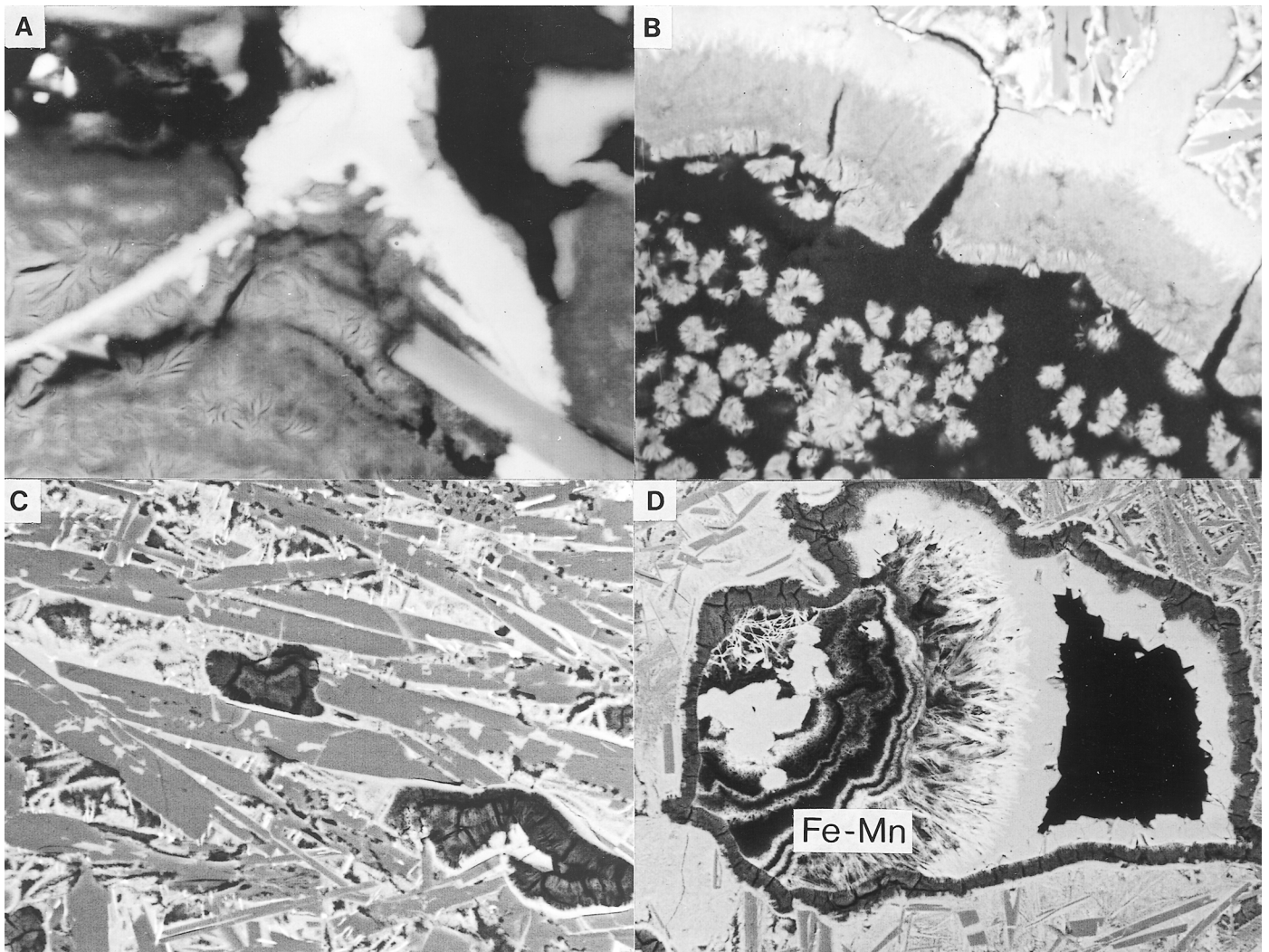


FIG. 7.—A) Back-scattered electron (BSE) image of mildly phosphatized glassy basalt. CFA (white) cross-cuts and embays smectite-replaced volcanic glass (mottled gray). Radial fibrous smectite (by EDS) ranges from Fe-poor (light gray regions) to Fe-rich (darker gray). Plagioclase lath (lower right, medium gray) is unaltered as indicated by its smooth, regular margins. *F7-86-HWD23-6*. Image width = 60 μm . B) BSE image of smectite-lined vesicle within phosphatized basalt. Fe-rich smectite (cream) lines vesicle and is in turn lined by two layers of Fe-poor smectite (dark and medium gray). Clusters of radial-fibrous Fe-poor, Mg-rich smectite (medium gray) partly fill vesicle (black). Within phosphatized basalt (upper right), glassy matrix is replaced by CFA (white) while plagioclase phenocrysts (gray laths) are unaltered. *L5-83-HW D5-A3-10*. Image width = 125 μm . C) BSE image of highly phosphatized basalt. Major CFA (white) and moderate fibrous smectite (dark gray) replace glassy groundmass within basalt, overprinting original basalt fabric. Plagioclase laths (medium gray) are Ca-rich, showing no sign of albitization. Note relict, subparallel Fe-Ti oxides (bright white north/south-oriented streaks). *L5-83-HW D5-A3-10*. Image width = 200 μm . D) BSE image of highly phosphatized basalt. CFA-replaced glass (white) surrounds partly dissolved plagioclase laths (light gray). Reticulate fabric within CFA (lower middle) reflects primary quench texture inherited from the volcanic glass during fabric-preservative CFA replacement. Vesicle is lined by a thin layer of CFA (white), which is in turn lined by phillipsite (dark gray). Botryoidal-fibrous Fe-Mn oxyhydroxides (black and white fibers and lamina filling left half of vesicle, labeled Fe-Mn) surround a nucleus of granular CFA (white). A final layer of blocky CFA (white) lines the remaining pore and passes into open pore space (black). *L5-83-HW D5-A3-10*. Image width = 450 μm .

smectite, and zeolite. Phosphatization is commonly more intense adjacent to fractures, large vugs, or sample surfaces and the intensity of mineralization diminishes gradually with distance from pore space. Locally, the pervasiveness of CFA precipitation changes abruptly across linear to undulating boundaries that roughly parallel fractures and/or vug boundaries. These observations suggest that the pervasiveness of phosphatization is partly dependent on rates of fluid exchange and seawater/rock ratios. In addition, diagenetic alteration of volcanic clasts to CFA can be fabric-preserving; thus primary sili-

cate textures locally play a crucial role in determining CFA replacement fabrics.

Mild phosphatization: Formation of palagonite, smectite, and CFA.—

Based on cross-cutting relationships, the earliest diagenetic stage in weakly phosphatized volcanic rocks is local palagonitization of volcanic glass followed by partial alteration of volcanic glass to Fe-poor smectite and CFA (Fig. 7A). Within regions of very mild phosphatization, CFA-filled fractures

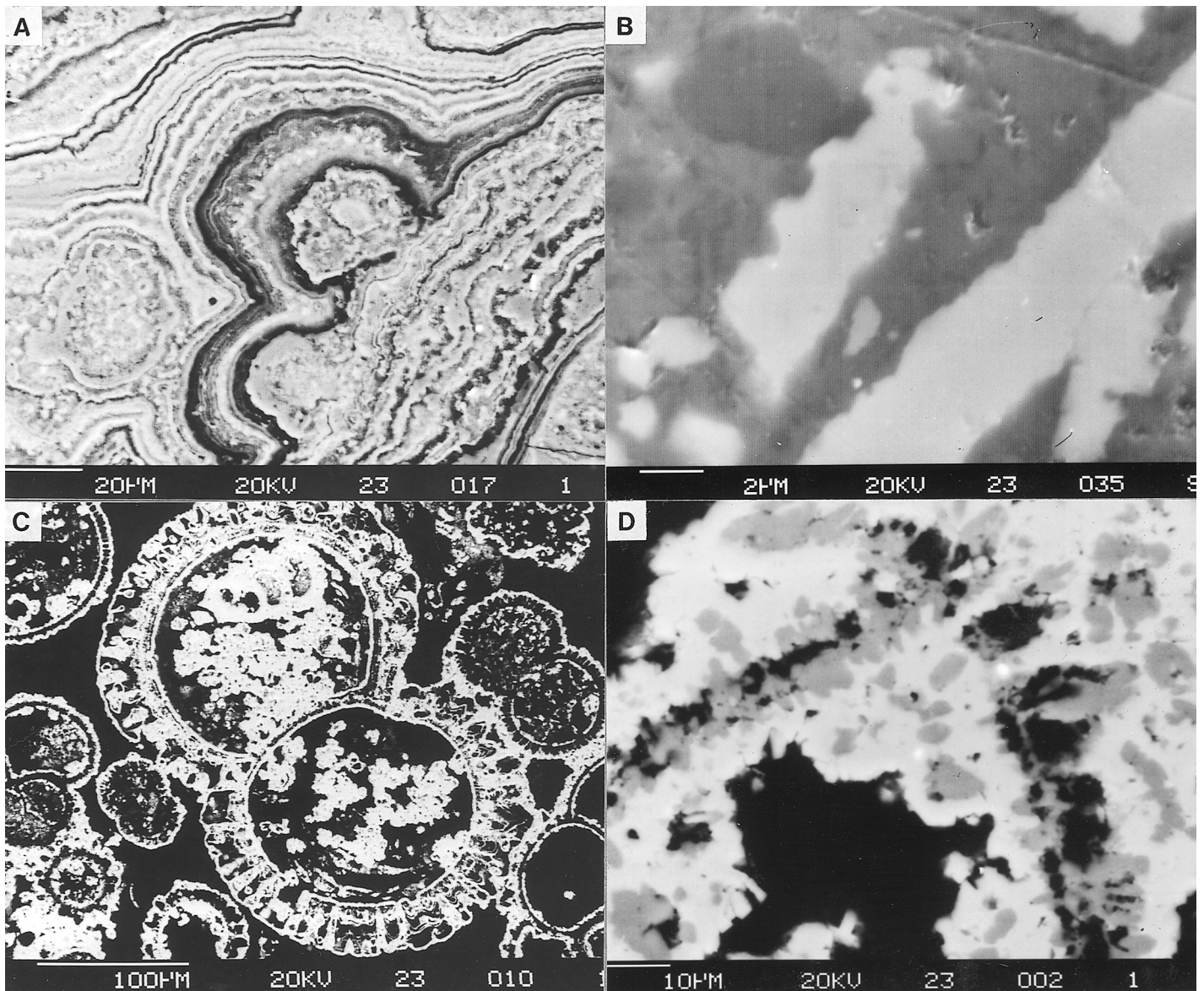


FIG. 8.—A) Back-scattered electron (BSE) image of vug-filling botryoidal CFA within phosphatized basalt. CFA (white and gray) forms botryoidal laminations separated by pore space (black) and surrounds minor Fe-Ti oxides (small bright white blebs). This atypical CFA texture may indicate CFA replacement of Fe-Mn oxyhydroxides or primary precipitation of CFA into pore space. *L5-83-HW D18-B3-7*. Image width = 200 μm . B) BSE image showing euhedral barite crystals (white) embayed by CFA (medium and dark gray). Medium and dark gray regions within CFA are compositionally indistinguishable by EDS analysis. *L5-83-HW D18-B3-7*. Image width = 22 μm . C) BSE image showing CFA molds (white) of foraminifera tests. Margins of molds are smooth and uniform, mirroring fine details of original test morphology and preserving original limestone fabric. *L5-83-HW D29-1A-A*. Image width = 500 μm . D) BSE image showing CFA coating (white) on partly replaced foraminifera test. Irregular and indistinct margins of CFA coating suggest partial CFA-replacement of carbonate (gray) before test partly dissolved to pore space (black). *L5-83-HW D18-B3-7*. Image width = 70 μm .

cross-cut smectite-replaced glass, indicating that smectite precipitation preceded precipitation of CFA.

Mild phosphatization is also typified by lining and partial filling of vugs and vesicles by smectite, CFA, and Fe-Mn oxyhydroxides. Vesicles are commonly lined by isopachous Fe-rich smectite (nontronite by EDS), followed by a layer of Fe-poor, Mg-rich smectite (Fig. 7B). Less commonly, Fe-poor smectite is followed by Fe-rich smectite; rarely multiple layers of isopachous smectite alternate between Fe-poor and Fe-rich. Many smectite-lined vugs and vesicles are subsequently lined or infilled by botryoidal Fe-Mn oxyhydroxides and/or micro-

crystalline to granular CFA. Sequences of vug-lining mineralization are highly variable both among and within samples.

Moderate to intense phosphatization: Smectite, zeolite, and CFA mineralization.—

In contrast to mildly phosphatized volcanic material where CFA commonly cross-cuts and embays smectite-replaced glass, moderately to intensely phosphatized volcanic glass is replaced by intergrown CFA and smectite. Relative amounts of CFA and smectite precipitation vary at the thin-section scale. In regions

of increased phosphatization, glass alters primarily to CFA and only secondarily to smectite (Fig. 7C). Within plagioclase-rich material, glass is also replaced by Ca-rich phillipsite (by EDS) and plagioclase is partly replaced by CFA.

Moderate to intense phosphatization can be either fabric-destructive or fabric-preservative. Within regions of complete replacement by fabric-destructive cryptocrystalline CFA, protolith identity is commonly discernible only through the presence of relict Fe-Ti oxide and/or local concentrations of cryptocrystalline smectite and zeolite. In regions of fabric-preservative phosphatization, CFA pseudomorphs primary protolith textures. Regions of reticulate CFA (Fig. 7D) and CFA growths on plagioclase laths resemble characteristic quench textures observed in MORB glass (Lofgren, 1974). Fine-scale preservation of primary silicate textures is surprising since CFA cannot replace silicate material through solid solution. Although the exact mechanism of replacement is unknown, fabric-preservative replacement of glass by CFA suggests coeval CFA precipitation and glass dissolution. Alternatively, phosphatization may have occurred through dissolution of glass to pore space (leaving an intact boxwork of microphenocrysts), infilling of resultant pores by CFA, later dissolution of microphenocrysts to pore space, and final infilling of phenocryst molds by CFA.

Vugs, vesicles, and fractures within moderately to intensely phosphatized volcanics are typically lined by abundant radial to euhedral phillipsite; cryptocrystalline or micro-granular CFA; and colloform or dendritic Fe-Mn oxyhydroxides (Fig. 7D). Sequences of void-filling phases vary widely, both among samples and within a single sample. In general, however, smectite, phillipsite, or Fe-Mn oxyhydroxides line pores, while Fe-Mn oxyhydroxides or CFA fill them. EDS analyses indicate that phillipsite occurring within vugs is largely K-rich, whereas phillipsite within glassy groundmass is most commonly Ca-rich. Local void-filling botryoidal CFA suggests that CFA may replace Fe-Mn oxyhydroxides (Fig. 8A), although CFA precipitation into open space can also form botryoids (D. Soudry, pers. commun., 1997).

Rarely occurring minerals.—

In addition to the major alteration phases discussed above, some phosphatized volcanic rocks also contain local occurrences of barite and, rarely, sparry calcite. Barite typically occurs within vugs and fractures as tiny euhedral laths disseminated in phosphatized detrital carbonate. Less commonly, veins are filled by a box work of pitted and embayed euhedral barite crystals within a CFA/smectite/phillipsite matrix. Those barite crystals commonly have scalloped edges, which suggests local CFA-replacement of barite (Fig. 8B).

Sparry calcite occurs within two breccia-conglomerates included in this study. Within those samples, clasts are cemented by partly phosphatized carbonate matrix. Dissolution cavities (< 75 mm across) within this matrix are partly to entirely filled by sparry calcite.

Two unidentified phases are locally present within phosphatized volcanic rocks. One breccia-conglomerate sample contains abundant CFA pseudomorphs of an unidentified mineral that is

morphologically similar to “dog tooth” calcite. In that sample, Fe-Mn oxyhydroxide encrusted CFA pseudomorphs extend isopachously from clast surfaces into CFA-replaced carbonate matrix. A second unidentified mineral, pseudomorphed by CFA, calcite, and phillipsite, is locally common. The unidentified crystals are twinned, chevron-shaped, and typically occur sandwiched between substrate and an enveloping Fe-Mn oxyhydroxide crust; rarely they fill voids. Chevron twinning and a square cross-section of crystals (when viewed down the apparent c-axis) suggest an original mineralogy of gypsum. Alternatively, while chevron twinning is not typical of zeolites, the mineral occurrence and square cross-section are indicative of phillipsite.

Phosphatization of Limestone

Phosphatized limestone is commonly associated with abundant Fe-Mn oxyhydroxides, phillipsite, and minor barite. Fe-Mn oxyhydroxides and phillipsite are especially common in limestone that is proximal to, or hosts, volcanic material. As discussed in detail below, while diagenetic mineralization sequences vary greatly within and among thin sections, petrographic and SEM analyses indicate that barite, Fe-Mn oxyhydroxides, and phillipsite generally precipitated both before and after phosphatization of the carbonate, and that the latter two also precipitated during phosphatization (Fig. 6). During phosphatization, calcite was dissolved and early-stage barite underwent local dissolution.

Early precipitation of accessory phases is indicated by their common dissemination within a massive CFA matrix, suggesting formation prior to occlusion and infilling of pore space by CFA. SEM images show CFA coatings on euhedral barite and phillipsite. Furthermore, phosphatized limestone commonly contains lithic fragments that are encrusted by Fe-Mn oxyhydroxides and phillipsite. These clasts were clearly encrusted prior to inclusion within the limestone, and therefore prior to phosphatization. The relative timing of precipitation among accessory phases is not determined due to lack of cross-cutting relationships.

Paragenesis during phosphatization.—

Within mildly phosphatized limestone, cryptocrystalline CFA occurs as a pore-lining phase and/or cement. In those rocks, massive CFA surrounds minor allochems and locally abundant foraminifera tests. Microcrystalline relict carbonate commonly imparts a sparkling birefringence to the CFA matrix and tests are partly to fully dissolved. Molds of foraminifera tests preserve original limestone fabric and their smooth margins mirror fine details of original test morphology (Fig. 8C). Fine-scale preservation of original limestone fabric precludes embayment or contemporaneous dissolution of carbonate and indicates that within regions of mild phosphatization, carbonate was not replaced by CFA.

In contrast, within moderately and intensely phosphatized limestone most carbonate dissolved and phosphatization appears to have occurred through both pore-lining and replace-

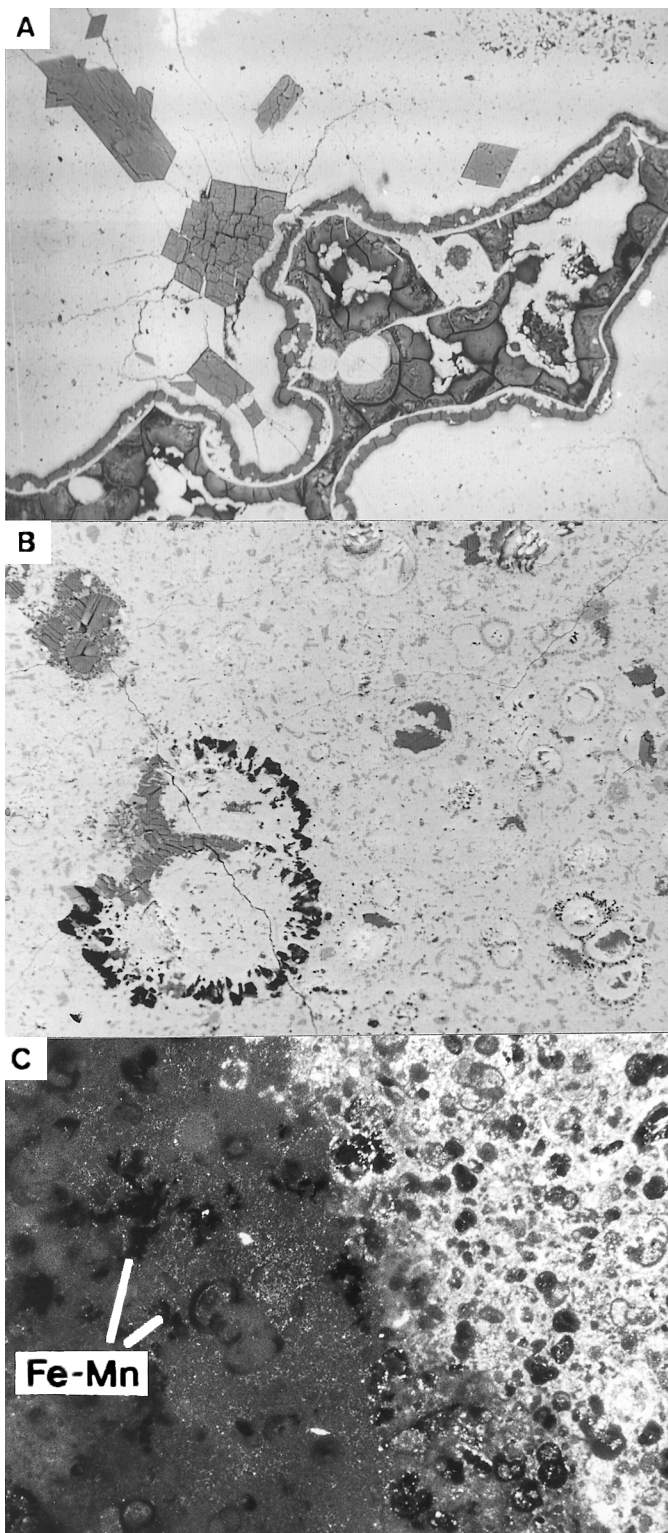


FIG. 9.—A) Back-scattered electron (BSE) image of K-rich phillipsite within phosphatized limestone proximal to an altered hyaloclastite fragment. Euhedral K-rich phillipsite (light gray, rhombohedrons and prisms) is supported by a massive CFA matrix (white). Hyaloclastite fragment (lower left corner extending to upper right) is replaced and lined by smectite (medium and dark gray) and CFA (white). *F7-86-HW D22-1C*. Image width = 500 μm . B) BSE image of CFA-replaced limestone with abundant microfossil tests. Relict carbonate tests (light gray) are surrounded by cryptocrystalline CFA (white), which commonly embays, and therefore replaces carbonate grain margins. Foraminiferal test (upper left) is infilled by phillipsite (dark gray); foraminiferal mold (black, lower left) is partly filled by phillipsite. *L9-84-CP D6-3*. Image width = 400 μm . C) Photomicrograph of phosphatized limestone under cross-polarized light. Dark-colored massive CFA contains common foraminiferal molds (very dark gray) and common disseminated dendritic Fe-Mn oxyhydroxides (labeled Fe-Mn). Unphosphatized carbonate on right is separated from the phosphatized region by an abrupt contact that cross-cuts foraminiferal tests, indicating a mineralization front. Minor relict microcrystalline carbonate (tiny white blebs at middle left) is more abundant within CFA that is closer to the unphosphatized region. *L5-83-HW D18-B3-7*. Image width = ~ 1.5 cm.

monly distinguishable from CFA matrix by color differences), which typically form through partial CFA-lining of moldic pores. Lamboy (1993) described this same sequence (CFA-lining of tests, carbonate-dissolution, CFA-infilling of molds) for the formation for CFA pseudomorphs in phosphatic carbonates from the Paris Basin and Peru shelf. In addition, CFA replacement of carbonate is indicated by local CFA embayments into allochem margins. Margins of molds within moderately and highly phosphatized limestone are commonly irregular and indistinct, suggesting partial CFA replacement prior to carbonate dissolution (Fig. 8D). Whether phosphatization occurs through authigenic (pore-lining) or diagenetic (alteration) processes, the resultant CFA fabric can preserve or overprint original protolith fabric.

Fe-Mn oxyhydroxides and phillipsite are common within moderately to highly phosphatized carbonates, especially in phosphatized limestone that is proximal to, or supports, volcanic material. Fe-Mn oxyhydroxides form abundant disseminated botryoids and dendrites; common euhedral K-rich phillipsite occurs as rosettes and solitary prisms (Fig. 9A). Less commonly, microcrystalline phillipsite and Fe-Mn oxyhydroxides pseudomorphed foraminifera by lining molds (Fig. 9B). The relative timing of precipitation between Fe-Mn oxyhydroxides and phillipsite is poorly constrained due to the lack of cross-cutting relationships. However, while phillipsite and CFA intergrowths are not observed, coprecipitation is likely because they coprecipitated within nearby phosphatized volcanic rocks.

Phosphatized volcanic-rich carbonate locally contains microcrystalline Fe-poor smectite disseminated within CFA groundmass and/or lining molds from dissolved hyaloclastite and basalt fragments. Within CFA-replaced groundmass, coprecipitated CFA and smectite are intergrown.

Moderately and highly phosphatized limestone is locally barite-rich. Barite typically occurs as small euhedral laths that are disseminated within a CFA (after carbonate) matrix. Common CFA embayments of barite indicate dissolution of barite during phosphatization.

ment processes. Dissolution of carbonate is indicated by foraminifera test molds or tests pseudomorphed by CFA. In addition, SEM images indicate that CFA matrix typically contains little relict carbonate.

Within severely to moderately phosphatized limestone, CFA reflects both pore-lining and replacement textures; one part of a test can be replaced while another is dissolved. Pore-lining is indicated by CFA pseudomorphs of foraminifera tests (com-

Post-phosphatization paragenesis.—

Post-phosphatization precipitation of barite, phillipsite, and Fe-Mn oxyhydroxides is indicated by SEM and petrographic analyses. Euhedral phillipsite nucleates on CFA and fills molds within CFA that are also commonly infilled by barite and Fe-Mn oxyhydroxides. Sparry calcite is rarely present within molds and large secondary dissolution vugs within CFA. Again, relative timing of precipitation between those phases could not be determined because cross-cutting relationships are lacking.

Mineralization fronts.—

CFA-replaced carbonate locally contains compositionally distinct domains that are separated by sharp boundaries. Domains are distinguishable by differences in crystallinity and by differences in abundances of CFA, Fe-Mn oxyhydroxides, barite, and/or relict carbonate. Boundaries between domains locally cross-cut foraminifera tests, suggesting that the boundaries are mineralizing fluid fronts rather than of depositional origin (Fig. 9C). These mineralization fronts are similar to those reported to occur in seamount silicified carbonates (Hein et al., 1981).

Locally, mineralization fronts broadly parallel voids, fractures, and/or outer surfaces of samples. Typically, regions adjacent to voids and surfaces are relatively enriched in CFA and Fe-Mn oxyhydroxides, indicating that mineralization fronts began at permeable openings and seawater entryways. Domains commonly have complex amoebae-like shapes. Those shapes most likely reflect multiple, overlapping fronts of mineralization and dissolution.

CONCLUSIONS

1. Phosphatization of both silicate and carbonate seamount protoliths occurs through precipitation in voids and through replacement. Regardless of protolith rock type, phosphatization can be either fabric-destructive or fabric-preserving. Within seamount phosphorites, direct molecular replacement of carbonate is not the most important process leading to fabric-preserving replacement by CFA. Rather, fabric-preserving CFA mineralization commonly occurred indirectly when CFA precipitated around microfossils, microfossil carbonate subsequently underwent dissolution, and finally further CFA precipitated in voids. This fabric-preserving phosphatization of carbonate was also described by Soudry and Lewy (1990) and by Lamboy (1993).
2. Fabric-preserving phosphatization of volcanic material is indicated by fine-scale replication of silicate fabrics within CFA. The precise mechanism of replacement is unknown, however solid-state substitution between CFA and silicate minerals clearly cannot occur. Fabric-selective phosphatization may have occurred through coeval CFA precipitation and glass dissolution, or alternatively through a process of cementation-dissolution-cementation analogous to that described for fabric-preserving phosphatization of limestone.
3. Phosphatization is most pervasive near sample surfaces, large pores, and fractures. Increased pervasiveness of phosphatization with increased proximity to fluid access routes suggests that fluid exchange rates and rock/water ratios are important controls on seamount phosphogenesis. It is likely that phosphatizing fluids were seawater-dominated. This interpretation is supported by diagenetic mineral assemblages that are typical of open-circulation, low-temperature seafloor alteration.
4. Breccia-conglomerates clearly show that CFA formed near the sediment-water interface because that is where reworked clasts can be shed from seamount flanks and redeposited within carbonate sediment. Occurrences of reworked phosphorite within a partly phosphatized matrix further indicate that phosphatization occurs over a relatively long time span, or occurs during several episodes separated by large time spans. Phosphatization on seamounts is a long-term process because phosphogenesis must encompass (1) initial phosphatization of limestone and/or volcanic material, (2) mass wasting and redeposition of phosphatized clasts, and (3) further phosphatization of carbonate matrix.
5. The mineral assemblage found in SMP deposits is characteristic of low-temperature seafloor weathering and implies that CFA precipitated hydrogenetically from seawater of ambient temperature. This interpretation is supported by microprobe analyses that indicate that dioctahedral, low-temperature smectite is intergrown with CFA (Benninger, 1998). In addition, oxygen isotopic analyses of CFA confirm a low-temperature origin for most Marshall and Johnston Island phosphorites (Hein et al., 1993). This finding is not surprising since the SMP deposits formed during Tertiary time when the Cretaceous seamounts were no longer hydrothermally active.
6. The close association between CFA and Fe-Mn oxyhydroxide precipitation suggests that similar to other low-productivity phosphorite deposits, SMP formation may have been facilitated by Fe-oxyhydroxide redox reactions. In seawater, Fe-oxyhydroxides have a weakly positive surface charge and can complex with phosphate ion (Roy, 1981). We suggest that phosphorus adsorbs onto surfaces of Fe-oxyhydroxide particles as they fall through the water column. Once within the oxygen minimum zone of suboxic Fe reduction, dissolution of Fe-Mn oxyhydroxides can release P and thereby increase phosphate concentration. Analogous to the Fe-P shuttle described for other low-productivity phosphorites (Jarvis, 1992; Schaffer, 1986; Lucas and Prévôt, 1985), Fe²⁺ released during Fe reduction may migrate to more oxic waters, reform oxyhydroxides, and again be available to shuttle P to (sub-oxic) phosphatization sites.
7. SMP formed within shallow sediment ponds and within sediment-free breccia and basalt where bacterially mediated anoxic diagenetic zones cannot have developed. Therefore, unlike other continental margin phosphorites that formed in bacterially mediated diagenetic zones within reducing sediments, SMP must have formed below a low-oxygen water column, probably within the oxygen minimum zone that invariably intersects the flanks of equatorial Pacific seamounts.

ACKNOWLEDGMENTS

This research was made possible through financial assistance from the U.S. Geological Survey Graduate Intern Program. Additional funding was provided by Sigma Xi, The Scientific Research Society (Grant-in-Aid of Research award #7143), and by the Geological Society of America and National Science Foundation (research award #4626-91). We are grateful to Leanne Roberts for providing invaluable technical support. We thank David Soudry and an anonymous reviewer for helpful comments.

REFERENCES

- ALT, J. C., 1995, Subseafloor processes in mid-ocean ridge hydrothermal systems, in Humphries, S., Zierenberg, R. A., Mullineaux, L. S., and Thompson R. E., eds., *Seafloor Hydrothermal Systems: Physical, Chemical, Biological and Geological Interactions*, Geophysical Monograph 91: Washington D.C., American Geophysical Union, p. 85-113.
- BATURIN, G. N., 1982, Phosphorites on the Sea Floor—Origin, Composition and Distribution, in *Developments in Sedimentology*, v. 33: New York, Elsevier Scientific Publishing Company, 343 p.
- BENNINGER, L. M., 1998, Distribution, origin, and diagenetic evolution of Pacific seamount phosphorite: M.S. Thesis, University of California, Davis, 82 p.
- BERSENEV, I. I., BATURIN, G. N., LELIKOV, E. P., AND GUSEV, V. V., 1990, Neogene phosphorites of the Sea of Japan, in Burnett, W. C., and Riggs, S. R., eds., *Phosphate Deposits of the World, Volume 3: Neogene to Modern Phosphorites*: Cambridge, Cambridge University Press, p. 167-176.
- BURNETT, W. C., CULLEN, D. J., AND MCMURTRY, G. M., 1987, Open-ocean phosphorites—in a class by themselves?, in Teleki, P. G., Dobson, M. R., Moore, J. R., and von Stackelberg, U., eds., *Marine Minerals: Advances in Research and Resource Assessment*: Dordrecht, D. Reidel Publishing Company, p. 119-134.
- CULLEN, D. J. AND BURNETT, W. C., 1986, Phosphorite associations on seamounts in the tropical southwest Pacific Ocean: *Marine Geology*, v. 71, p. 215-236.
- HEIN, J. R., VALLIER, T. L., AND ALLAN, M. A., 1981, Chert petrology and geochemistry, Mid-Pacific Mountains and Hess Rise, Deep Sea Drilling Project Leg 62, in Thede, J., Vallier, T. L., eds., *Initial Reports of the Deep Sea Drilling Project*, v. 62: Washington, U. S. Government Printing Office, p. 711-748.
- HEIN, J. R., ET AL., 1990, Geological, geochemical, geophysical, and oceanographic data and interpretations of seamounts and Co-rich ferromanganese crusts from the Marshall Islands, KORDI-USGS, R.V. *Farnella*, Cruise F10-89-CP, U.S. Geological Survey Open File Report 90-407, 246 p.
- HEIN, J. R., YEH, H. W., GUNN, S. H., SLITER, W. V., BENNINGER, L. M., AND WANG, C. H., 1993, Two major Cenozoic episodes of phosphogenesis recorded in equatorial Pacific seamount deposits: *Paleoceanography*, v. 8, p. 293-311.
- HONNOREZ, J., 1981, The aging of the oceanic crust at low temperature, in Emiliani, E., ed., *The Sea: the Oceanic Lithosphere*, v. 7: New York, John Wiley and Sons, p. 525-587.
- JACKSON, E. D., ET AL., 1980, *Proceedings of the Ocean Drilling Program, Initial Reports*, v. 55: Washington, U.S. Government Printing Office, Ocean Drilling Program, 868 p.
- JARVIS, I., 1992, Sedimentology, geochemistry and origin of phosphatic chalks: The Upper Cretaceous deposits of NW Europe: *Sedimentology*, v. 39, p. 55-97.
- KAYEN, R. E., SCHWAB, W. C., LEE, H. J., TORRESAN, M. E., HEIN, J. R., QUINTERNO, P. J., AND LEVIN, L. A., 1989, Morphology of sea-floor landslides on Horizon Guyot: application of steady-state geotechnical analysis: *Deep-Sea Research*, v. 36, p. 1817-1839.
- LAMBOY, M., 1993, Phosphatization of calcium carbonate in phosphorites: microstructure and importance: *Sedimentology*, v. 40, p. 53-62.
- LOFGREN, G. E., 1974, An experimental study of plagioclase crystal morphology: isothermal crystallization: *American Journal of Science*, v. 274, p. 243-273.
- LUCAS, J., AND PRÉVÔT, L., 1985, The synthesis of apatite by bacterial activity: mechanism, in Lucas, J., and Prévôt, L., eds., *Phosphorites: Sciences Géologiques Mémoire*, v. 77, p. 83-92.
- O'BRIEN, G. W., AND HEGGIE, D., 1988, East Australian continental margin phosphorites: *EOS*, v. 69, p. 2.
- O'BRIEN, G. W., MILNES, A. R., VEEH, H. H., HEGGIE, D. T., RIGGS, S. R., CULLEN, D. J., MARSHALL, J. F., AND COOK, P. J., 1990, Sedimentation dynamics and redox iron-cycling: controlling factors for the apatite-glaucinite association of the east Australian continental margin, in Notholt, A. J. G., and Jarvis, I., eds., *Phosphorite Research and Development*: London, Geological Society of London Special Publication 52, p. 61-86.
- PREMOLI-SILVA, I., ET AL., 1993, *Proceedings of the Ocean Drilling Program, Initial Reports*, v. 144: College Station, Texas, Ocean Drilling Program, p. 145-312.
- ROY, S., 1981, *Manganese Deposits*: London, Academic Press, 458 p.
- SAGER, W. W., WINTERER, E. L., FIRTH, J. V., ET AL., 1993, *Proceedings of the Ocean Drilling Program, Initial Reports*, v. 143: College Station, Texas, Ocean Drilling Program, p. 273-288.
- SCHAFFER, G., 1986, Phosphatic pumps and shuttles in the Black Sea: *Nature*, v. 321, p. 515-517.
- SCHWAB, W. C., LEE, H. J., KAYEN, R. E., QUINTERNO, P. J., AND TATE, G. B., 1988, Erosion and slope instability on Horizon Guyot, Mid Pacific Mountains: *Geo-Marine Letters*, v. 8, p. 1-10.
- SOUDRY, D., AND LEWY, Z., 1990, Omission—surface incipient phosphate crusts on early diagenetic calcareous concretions and their possible origin, upper Campanian, southern Israel: *Sedimentary Geology*, v. 66, p. 151-163.
- THOMPSON, G., 1983, Basalt-seawater interaction, in Rona, P. A., Bostrom, K., and Smith, K. L., eds., *Hydrothermal Processes at Seafloor Spreading Centers*: New York, Plenum, p. 225-278.